$kT < t_1 < T$ and $0 < m < 1$. Define m as the current filling factor. After mathematical manipulation,

$$m = \frac{1}{\xi} = \frac{M^2}{k\dfrac{R}{2fL}}. \tag{13}$$

From the above equation, we can see that the DCM is caused by the following factors.

- Switching frequency f is too low.
- Duty cycle k is too small.
- Inductance L is too small.
- Load resistor R is too big.

In the DCM, current i_L increases during switch-on and decreases in the period from kT to $(1-k)mT$. The corresponding voltages across L are V_I and $-(V_C - V_I)$. Therefore,

$$kTV_I = (1-k)mT(V_C - V_I).$$

Hence,

$$V_C = \left[1 + \frac{k}{(1-k)m}\right] V_I. \tag{14}$$

Since all C, C_1, and C_O are large,

$$V_O = V_C = V_{CO} = \left[1 + \frac{k}{(1-k)m}\right] V_I$$

or

$$V_O = \left[1 + k^2(1-k)\frac{R}{2fL}\right] V_I. \tag{15}$$

The voltage transfer gain in the DCM is

$$M_{DCM} = 1 + k^2(1-k)\frac{R}{2fL}. \tag{16}$$

The relation between dc voltage transfer gain M and the normalized load at various k in the DCM is also shown in Fig. 2(f). We can see that, in DCM, the output voltage increases as the load resistance R is increasing.

III. SIMULATION AND EXPERIMENTAL RESULTS OF SELF-LIFT CUK CONVERTER

A. Simulation Results

Microsim Design Center (including PSPICE) is a standard electronic circuit simulation software package. Using the Design Center 8 (Evaluation Version) to simulate the proposed new dc–dc converters is a helpful method for circuit design. In the simulation, the switch is an NMOS IRF540 and the diode is an MR824. The other parameters are: $R = 30\ \Omega$, $k = 0.4$, $C = C_1 = C_O = 100\ \mu$F, and $L = L_O = 100\ \mu$H. Input voltage is $V_I = 30$ V. The simulation waveforms are shown in Fig. 3(a). From the simulation waveforms, we can see that the output voltage is essentially a dc voltage.

B. Experimental Results

A particular breadboard prototype of the proposed self-lift Cuk converter was constructed. The semiconductor switch S is an NMOS IRFP460. The diode is an MR824. The other parameters are: $R = 30$–$340\ \Omega$, $k = 0.1$–0.9, $C = C_O = 100\ \mu$F, and $L = 470\ \mu$H. Input voltage is $V_I = 0$–30 V. The experimental waveforms shown in Fig. 3(b) are: channel 1 of the oscilloscope is the pulsewidth modulation (PWM) switching signal, and channel 2 is the output voltage. It can be seen that the output voltage is essentially a dc voltage. There are spikes in the switching point because the PWM signal is not ideal and the components are not ideal.

IV. CONCLUSIONS

This letter has introduced the skills of the voltage lift technique applied in the design of dc–dc converters. A group of new dc–dc step-up (boost) converters—six self-lift converters— has been developed by applying the voltage lift technique. These converters are different from the conventional converters, and have higher output voltage and better characteristics. They will be used in consumer engineering projects and industrial applications.

REFERENCES

[1] F. L. Luo, "Positive output Luo-converters: Voltage lift technique," *Proc. IEE—Elect. Power Applicat.*, vol. 146, no. 4, pp. 415–432, July 1999.
[2] ——, "Negative output Luo-converters: Voltage lift technique," *Proc. IEE—Elect. Power Applicat.*, vol. 146, no. 2, pp. 208–224, March 1999.
[3] F. L. Luo and H. Ye, "Self-Lift DC–DC Converters," in *Proc. 2nd IEEE Int. Conf. PEDES'98*, Perth, Western Australia, Nov. 30–Dec. 3, 1998, pp. 441–446.
[4] F. L. Luo, "Re-lift converter: Design, test, simulation and stability analysis," *Proc. IEE—Elect. Power Applicat.*, vol. 145, no. 4, pp. 315–325, July 1998.
[5] D. Maksimovic and S. Cuk, "Switching converters with wide DC conversion range," *IEEE Trans. Power Electron.*, vol. 6, pp. 151–157, Jan. 1991.
[6] Y. Liu and P. C. Sen, "New class-E DC–DC converter topologies with constant switching frequency," *IEEE Trans. Ind. Applicat.*, vol. 32, pp. 961–969, July/Aug. 1996.
[7] R. P. Massey and E. C. Snyder, "High voltage single-ended DC–DC converter," in *Proc. IEEE PESC'77*, 1977, pp. 156–159.

Strategy and Implementation for Design and Analysis of Induction Machines Supplied by Power Electronic Inverters

C. C. Chan, Zhengming M. Zhao, S. Meng, Y. F. Liu, and E. W. C. Lo

Abstract—Induction machines supplied by power electronic inverters for variable-speed systems are different from those fed directly from a utility power line. The design strategies of induction machines considering power electronic supply are presented and implemented. The proposed approach permits the integration of the design of machines with inverters, comprehensive performance analysis, and system optimization.

Index Terms—Induction machine, integration design, inverter drive.

I. INTRODUCTION

Inverter-driven induction machines (IDIMs) are the prime choice of variable-speed drives in a wide field of applications due to their low

cost, simple and rugged construction, high reliability, minor maintenance, and well-developed control algorithms. However, the major attention had been given to the development of solid-state inverters and control algorithms before, and the induction machines themselves had not undergone any profound changes compared to the solid-state inverter counterpart within the same system. Thus, the variable-speed systems, particularly, high-speed drives and large machines still have the problems of low power factor, low efficiency, and poor utilization of the inverter. In fact, with an inverter as the power supply, the operational conditions of an induction machine are much different from the conventional supply with fixed voltage and frequency, which implies that the design of induction machines should be reconsidered to make them more suitable for the inverter-driven variable-speed systems.

II. OPERATION CONDITIONS AND DESIGN STRATEGIES

The remarkable deference between the inverter supply and the utility line supply of an induction machine is that the former can change its frequency and input voltage flexibly, whereas the latter only provides a fixed frequency and voltage. With an adjustable frequency, an induction machine is able to move its torque–speed profile from the rated synchronous frequency to any other frequencies of interests. This movable torque–speed profile ensures that the line startup performance of an induction machine under a fixed synchronous frequency and other considerations become unnecessary. Essentially, it is possible that the line-start torque can be replaced by the peak torque, and also the rated torque can be set at a most favorable slip frequency, resulting in minimized slip power losses and stray iron losses.

Different from the conventional design of an induction machine, the new design strategies put appropriate steady-state characteristics in the first consideration other than the startup characteristics, which implies that the restrictions imposed by rotor slot shape can also be lifted. The design with inverter-driven condition allows the stator and rotor slot numbers, shapes, and size to be optimized exclusively for minimizing the leakage inductance and resistance. Also, the effective utilization of rotor slot area can be increased. Consequently, increased peak torque, improved efficiency, and power factor can be expected.

III. DESIGN AND EXPERIMENTAL COMPARISONS

To compare the difference between an inverter-driven machine design and a conventional machine design, two induction machines are designed and tested with same outer dimensions. Motor 1 is designed using the conventional method, and Motor 2 using proposed IDIM strategies. Table I shows the major design results of the conventional (Motor 1) and the IDIM (Motor 2).

As compared to Motor 1, Motor 2 has the same stator outer/inner diameters and effective length, but the stator slot number, rotor slot number, rotor slot dimensions, and shape are noticeably different. The rotor slot depth of Motor 2 is decreased by about 20%, and the width increased by about 15%, resulting in a reduction of rotor resistance by 19% and rotor leakage inductance by 17%. In addition, the active iron and copper ratio and the numbers of stator and rotor slot in Motor 2 are optimized for maximum output power.

The practical test set consists of an IDIM, a torque–speed sensor, a variable-speed gear box, a dc generator, a load box, and a 25-kVA converter. The real test site is shown in Fig. 1.

Driven by the same inverter, the performance of Motor 1 and the performance of Motor 2 are tested and compared. Table II summarizes the results at their rated power, no-load, and short-circuit operation conditions.

It is seen from Table II that, at the rated point, the efficiency, power factor, and temperature rise of the two motors are almost the same. However, the output power of Motor 2 is, significantly, 25% greater

TABLE I
COMPARISON OF DESIGN RESULTS

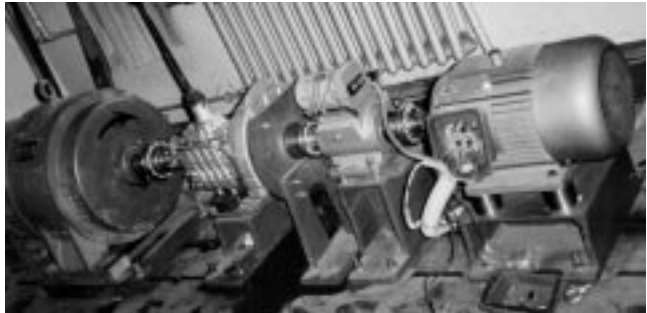|	Motor 1	Motor 2	Unit
Stator D_o/D_i	260 / 170	260 / 170	(mm)
Core length	150	150	(mm)
Airgap length	0.5	0.5	(mm)
Stator slot	44	48	
Rotor slot	36	38	
x_1/r_1	0.77 / 0.3126	0.71 / 0.3005	(Ω)
x_m	46.37	52.39	(Ω)
x_2/r_2	0.76 / 0.3111	0.63 / 0.2520	(Ω)
Stator /rotor iron	24.42 / 16.15	21.32 / 15.39	(kg)
Stator /rotor copper	10.67 / 6.53	12.85 / 7.01	(kg)

Fig. 1. Test site of Motor 2.

than that of Motor 1 and the maximum torque of Motor 2 is almost 1.2 times greater than that of Motor 1. The figures imply that, if the two motors are designed with the same rated power, the size of Motor 2 will be about 25% smaller than that of Motor 1. In addition, the no-load current (I_o) of Motor 2 is about 13% smaller than that of Motor 1, which means that the passive power required by Motor 2 is less than that of Motor 1 due to larger x_m and smaller x_2 in Motor 2.

Another comparison is done under constant-torque condition; the tow motors were tested for variable-speed performance under varying input frequency. The results of the comparison are shown in Figs. 2 and 3 with a constant torque of 77 N·m. Obviously, the efficiency and power factor of Motor 2 could be maintained at high values in a wide frequency range, while Motor 1 could achieve this only at the rated frequency. This is a major benefit from the proposed IDIM design strategies for variable-speed systems.

IV. CONCLUSIONS

From the above design, analysis, and experimental comparisons, we conclude the following.

1) The main reason of having room to improve the IDIM design is that the design is now free from the restriction imposed by the line startup performance requirements. The variable frequency provided by the inverter allows the design to be more focused on the performance in quasi-steady-state conditions and system optimization.
2) Being freed from line-start requirements, the rotor slot number, shape, and size are to be reconsidered. The optimal design of rotor slots results in improved maximum torque, rated slip, and efficiency.

TABLE II
COMPARISON OF PERFORMANCE

	Motor1	Motor2	Unit		Motor1	Motor2	Unit
Rated power	12	15	kW	Temp. rise	42.38	44.65	C
Speed	1464	1465	Rpm	T_{max}(at $V=V_n$)	181.6	218.8	N. m
Phase voltage	220	220	Volts	T_s (at f=5 Hz)	102	90	N. m
Stator current	20.17	25.03	Amp	I_o (at V= Vn)	8.1	7.1	Amp
Power factor	0.901	0.908		I_s (at f =5 Hz)	39.1	38.0	Amp

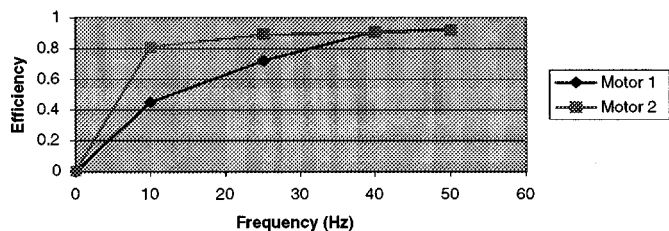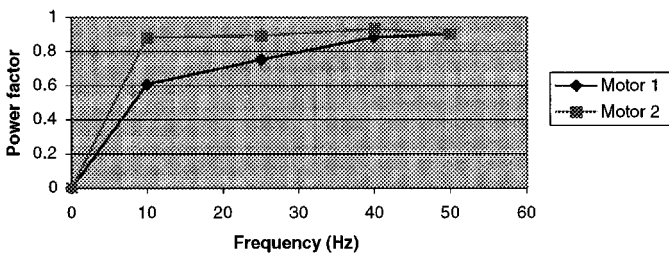Fig. 2. Comparison of efficiency.

Fig. 3. Comparison of power factor.

3) If an induction machine is designed in accordance with the above strategies, it is possible to increase output power by 20%–30% without sacrificing the size and performance.

REFERENCES

[1] N. P. Nee, "Rotor slot design of inverter-fed induction motors," in *Proc. IEE Electrical Machines and Drives Conf.*, Sept. 1995, pp. 52–56.
[2] Y. Akiyama *et al.*, "A study of the most suitable design of inverter-driven induction motors," *PCIM*, pp. 38–44, June 1994.
[3] Z. M. Zhao, L. Y. Xu, and A. El-Antably, "Strategies and a computer aided package for design and analysis of induction machines for inverter-driven variable speed systems," in *Conf. Rec. IEEE-IAS Annu. Meeting*, Oct. 1995, pp. 523–529.
[4] S. Williamson and C. I. McClay *et al.*, "Optimization of the geometry of closed rotor slot for cage induction motors," *IEEE Trans. Ind. Applicat.*, vol. 32, pp. 560–568, May/June 1996.
[5] A. Barbour and W. T. Thomson, "Finite element study of rotor slot designs with respect to current monitoring for detecting static airgap eccentricity in squirrel-cage induction motors," in *Conf. Rec. IEEE-IAS Annu. Meeting*, Oct. 1997, pp. 112–119.

Adaptive Control of Robot Manipulators Using Fuzzy Neural Networks

Yang Gao, Meng Joo Er, and Song Yang

Abstract—This letter presents an adaptive fuzzy neural controller suitable for multilink manipulators motion control. The proposed controller has the following salient features: 1) self-organizing fuzzy neural structure; 2) online learning of the robot dynamics; 3) fast convergence of tracking error; and 4) adaptive control. Computer simulation results of a two-link manipulator demonstrate that excellent tracking performance can be achieved under external disturbances.

Index Terms—Adaptive control, fuzzy neural networks, multilink manipulators.

I. INTRODUCTION

Design of robust adaptive controllers for robot manipulators is one of the most challenging tasks for control engineers nowadays, especially when manipulators are required to maneuver very quickly under external disturbances. In the last few decades, much research effort has been put into the design of model-free adaptive intelligent controllers using fuzzy logic and neural networks. However, most adaptive fuzzy controllers have difficulties in determining suitable fuzzy control rules and membership functions [1]. If the number of fuzzy rules is large, real-time implementation will be difficult or impossible. Recently, hybrid control laws containing neural networks (NNs) have attracted more and more attention. In [2]–[4], NNs were successfully used to approximate highly nonlinear dynamics of robot manipulators so as to achieve adaptive control.

All these existing fuzzy or/and neural control methods require predefined and fixed fuzzy rules or NN structure, which reduces the flexibility and numerical processing capability of the controller. More importantly, it results in redundant or inefficient computation. Unlike most of these existing intelligent control schemes, our proposed adaptive fuzzy neural controller (AFNC) offers a novel learning algorithm, termed the dynamic fuzzy neural network (D-FNN) algorithm, which can recruit or delete fuzzy control rules automatically and